

Spike discrimination using amplitude measurements with a low-power CMOS neural amplifier

(Invited Paper)

Timothy Horiuchi*, Dorielle Tucker†, Kevin Boyle‡, and Pamela Abshire*

*Dept. of Electrical & Computer Engineering, Institute for Systems Research, and Neuroscience and Cognitive Science Program, University of Maryland, College Park, MD 20742, USA

Email: {timmer, pabshire}@umd.edu

†Dept. of Electrical Engineering, University of South Florida, Tampa, FL 33620, USA

‡Dept. of Electrical Engineering & Computer Science, Massachusetts Inst. of Tech., Cambridge, MA 02139, USA

Abstract—Integrated CMOS neural amplifiers have recently grown in importance as large microelectrode arrays have begun to be practical. We previously reported low-power neural amplifiers with integrated pre-filtering and measurements of the spike signal to reduce data bandwidth and to facilitate spike-sorting prior to transmission to a data-acquisition system. Characteristics of a prototype circuit were reported using a 1.5 V power supply, suitable for single cell battery operation. Here we report improved transient amplitude tracking as well as application of the circuit in live recordings of wide-field motion sensitive cells in blowflies. The features extracted by the chip efficiently discriminate between stimulus conditions, as demonstrated by receiver operating characteristic analysis.

I. INTRODUCTION

Integrated biosignal amplifiers have been designed and reported for different combinations of constraints such as low-noise, low-frequency, low-power, low-voltage, and zero-DC gain [1]–[9]. The primary application motivating this work is neural recordings from small animals in flight; as a result, much of our design is constrained by the use of a single cell battery (1.5 V) to reduce system weight. We achieve this by using CMOS transistors in or near the subthreshold region of operation. In addition to low power operation, subthreshold operation allows the transistors to work with lower gate-to-source and drain-to-source voltages while remaining in saturation.

The low power amplifier, peak detector, and trough detector were previously described in [10]; here we report extended analysis, measurements, and use of the circuit for spike discrimination. A block diagram of system components is shown in Fig 1. The system accepts signals from differential electrode inputs and produces several output signals, including the amplified waveform as well as its upper and lower envelope and level crossings. The design of the amplifier is based on a capacitive feedback approach as described by Harrison and Charles [1]. Following the amplifier, we have implemented a peak detector, a trough detector, and a level comparator to detect and measure the amplitude of the spike signal.

II. PRECISION OF FEATURE MEASUREMENTS

The peak and trough detectors are shown in Figure 2, and were previously described in [10]. The peak detector produces an output voltage that quickly follows positive transients in the input signal, whereas for negative transients transistor M4 turns off and the output voltage is slow rate limited by a small leak current. The trough detector behaves similarly with the roles of positive and negative transients reversed.

The peak and trough detector circuits suffer from systematic errors such as finite amplifier gain and parasitic capacitance coupling in addition to dynamic-range limits. Due to the voltage requirements of the peak and trough detector circuits, both peak and trough values

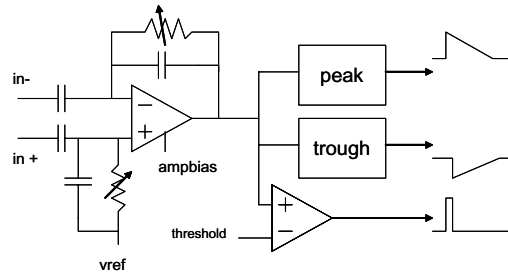


Fig. 1. Block diagram of the neural amplifier and amplitude circuits.

saturate for large input signals, limiting the dynamic range of the encoding. The peak and trough detectors are effectively asymmetric voltage-followers where the amplifier gain and output offset voltage play a role in the final output. The amplifier’s voltage characteristic can be stated as:

$$V_A = V_o + A(V_+ - V_-) \quad (1)$$

where V_A is the amplifier’s output voltage, V_o is the output offset voltage, A is the amplifier gain, and $V_{+,-}$ are the differential inputs. The rectifying elements for peak and trough detection are nFET and pFET source-followers, respectively, and we can find the steady-state output voltages, $peakout$ and $troughout$, as a function of the input, V_{input} . The steady state output voltage for the peak detector is:

$$peakout = \frac{\kappa A V_{input}}{\kappa A + 1} + \frac{\kappa V_o - V_T \ln\left(\frac{I_{bias}}{I_o}\right)}{\kappa A + 1} \quad (2)$$

where κ is the subthreshold slope factor, V_{input} is the differential input signal, V_T is the thermal voltage, I_{bias} is the source follower bias current, and I_o is the pre-exponential scaling current for sub-threshold operation. In the case of large amplifier gain, the first term dominates and the peak detector output is close to the desired value. Similarly, the trough detector produces a steady-state output voltage equal to:

$$troughout = \frac{A V_{input}}{A + 1} + \frac{V_o}{A + 1} + \frac{V_T}{\kappa(A + 1)} \cdot \ln\left(\frac{I_{bias}}{I_o}\right) \quad (3)$$

With sufficient amplifier gain, the gain errors are minimal, leaving only an offset error. But how quickly can we reach steady-state? With a significant difference between the input and the capacitor voltage, the circuits respond quickly, but as the difference approaches zero, the current drops. In the peak detector circuit, using the small-signal output resistance of the source-follower that is reduced by the

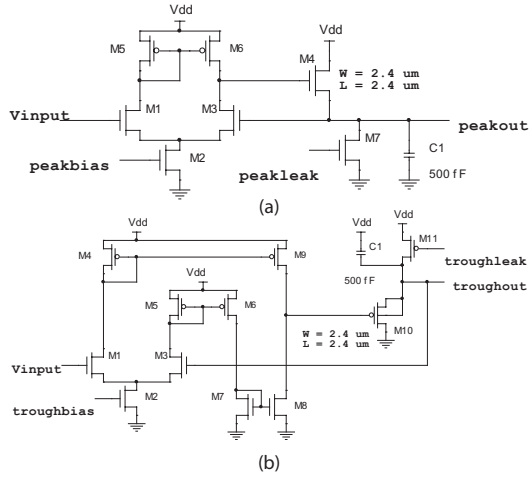


Fig. 2. "Zero-offset" peak detector circuit with a variable decay rate set by parameter *peakleak*.

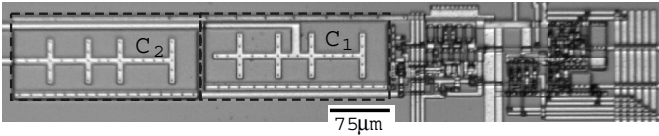


Fig. 3. Die photo of the fabricated circuit, comprising amplifier, level detector, and peak/trough detector circuits.

amplifier gain, we find a time constant,

$$\tau = R_{\text{sourcefollower}} \cdot C = \frac{C}{g_m \cdot A} \quad (4)$$

where C is the capacitance between the negative differential input and the negative terminal of the amplifier. The transconductance g_m is determined by the current I_{bias} , thus a rapid response in peak and trough measurements requires higher current.

In addition to the expected DC errors, parasitic capacitance in the rectifying elements also affects the peak and trough measurements. When the input voltage drops below the peak voltage, the amplifier output drops suddenly towards ground and the parasitic capacitance pulls the peak detector output voltage down by a fraction of the amplifier's voltage drop.

III. CHIP MEASUREMENTS

The circuit layout occupies about 91,000 μm^2 , dominated by the two 10 pF input capacitors. The chip was fabricated in a 1.5 μm double-poly, double-metal process. Fig 3 shows a photomicrograph of the fabricated circuit, with input capacitors at the left, amplifier to the right of the capacitors, and level/peak/trough detectors at the right. Although the amplifier was designed for a gain of 40 dB, the measured midband voltage gain is approximately 42.5 dB (gain = 133). Parameters *ampbias* and *rbias* independently control the low-frequency and high-frequency corners for the bandpass characteristics of the amplifier. Transfer characteristics were shown in [10] and are not repeated here.

A. Noise

We measured the noise spectral density at the output of the amplifier using a network analyzer (Agilent 4395A) and computed the input-referred values by dividing each noise measurement point by the measured gain at the closest measured frequency (Fig 4). By integrating under the noise spectral density curve from 10 Hz to 10

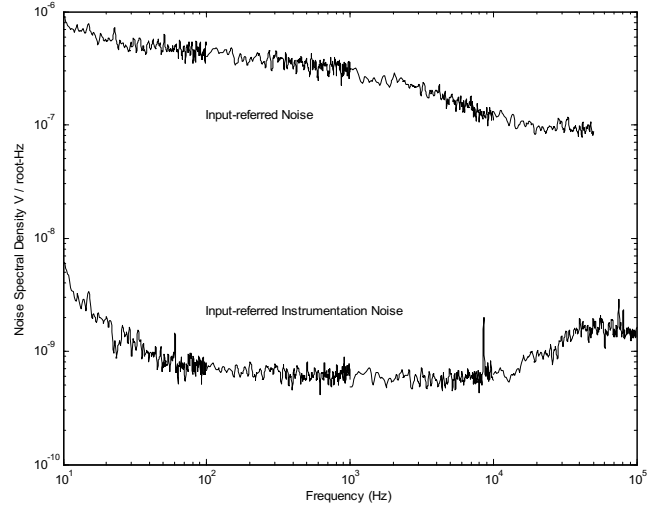


Fig. 4. Noise spectral density for the neural amplifier with parameters: *ampbias* = 0.610 V and *rbias* = 1.27 V.

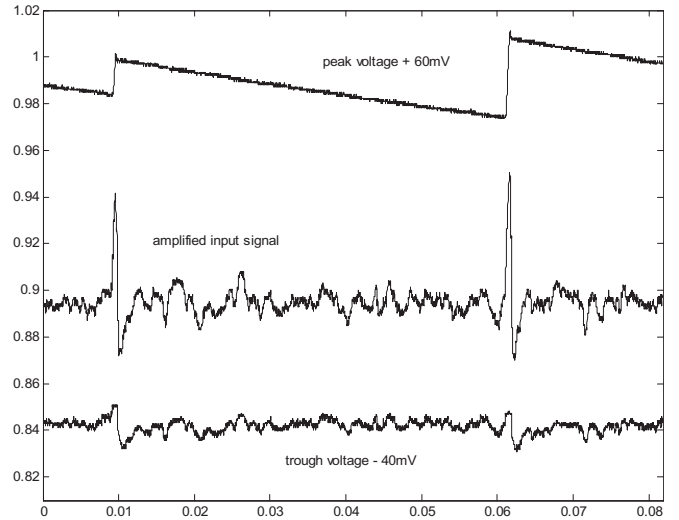


Fig. 5. Peak and trough detectors (top and bottom traces) respond to a spike input when $V_{\text{dd}}=1.5$ V.

kHz we obtain a total input-referred rms noise voltage of 20.6 μV rms, for *ampbias* = 0.610V, *rbias* = 1.27V, and $V_{\text{dd}} = 1.5$ V.

B. Peak-to-Trough Measurement

We tested the peak and trough detector circuits with pre-recorded ferret cortex signals obtained from the Neural Systems Laboratory at the University of Maryland. Signals were played to the chip using an arbitrary waveform generator (Agilent 33120A) with an attenuator to scale the signals to physiological levels. Fig 5 shows an example of the outputs for two input spikes and the resulting response from peak and trough circuits for $V_{\text{dd}} = 1.5$ V. The peak detector output has been shifted upwards by 60 mV and the trough detector output downwards by 40 mV for clarity. The trough detector output experiences significant signal coupling due to the gate-well capacitance in the rectifying transistor. For positive transients of the input signal, this parasitic capacitance pulls the trough detector output up with the amplifier output by 10-20 mV before the pFET turns off. The decay rate of the peak detector was set relatively low and the

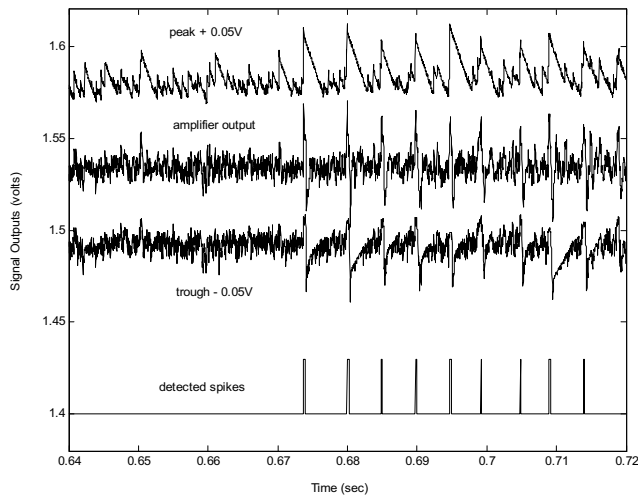


Fig. 6. Direct neural recording from a blowfly wide-field horizontal motion-sensitive cell (H1) showing, from top to bottom, the outputs of the peak detector, amplifier, trough detector, and comparator.

trough decay rate set relatively high. The decay rates need not remain constant, however, and in practice, the peak and trough values would be sampled following a spike, prior to resetting the values quickly by transiently boosting the decay rates.

C. Live blowfly recordings

We also tested the circuits by recording from neurons in the blowfly (*Sarcophaga*) visual system (H1 and HS, wide-field horizontal motion-sensitive cells) to demonstrate the high-impedance inputs of the chip and DC-isolation provided by the input capacitors. Fig 6 shows an example recording from the fly, showing the amplifier, peak detector, trough detector, and (processed) comparator outputs. Due to the circuit's limited dynamic range with a 1.5 V power supply, in these experiments we used a 3 V power supply to better demonstrate the response of the feature detectors. The output of the peak detector has been shifted up by 50 mV for clarity, and the output of the trough detector has been shifted down by 50 mV. The amplifier output represents the measured values, and the comparator output has been processed to show the times of the detected spikes for a given threshold.

D. Spike Discrimination

We further investigated the ability of the feature detectors to provide information for spike sorting. Using a visual stimulus that periodically changed its direction of motion, neural activity was recorded and spike amplitude information was computed offline from the peak and trough measurements taken at specific times following the level detector output signal. For comparison, we also used a software-based peak and trough detector algorithm (using MATLAB [11]) which measured the maximal (peak) and minimal (trough) voltages of the amplified waveform occurring anytime within 2.0 milliseconds following a spike-detection. Fig 7(a) shows the amplified signal for different directions of visual motion (arrows), Fig 7(b,c) show the measured spike-amplitudes as a function of time and Fig 7(d,e) show histograms of the measured spike-amplitudes. The amplified waveform clearly shows differences in waveform trough values in the different pattern directions, suggesting that the waveforms in the two conditions are produced by different neurons. Comparison of spike-amplitude measurements as determined in software and the chip further confirm the existence of distinct neuron classes. The spikes observed under the two stimulus conditions are segregated into classes corresponding to opposite directions of motion and shown

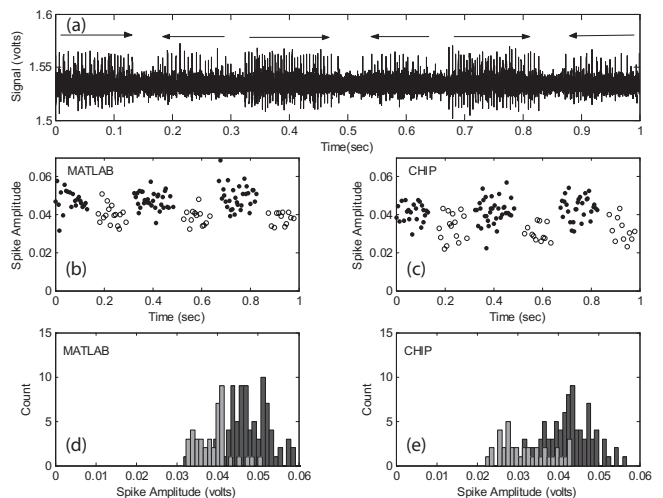


Fig. 7. Neural responses elicited by a visual stimulus moving in two alternating directions. (a) The amplified waveform. (b,c) Spike-amplitude measurements determined by software (b) and the chip (c), with spikes corresponding to rightward (leftward) stimuli shown as filled (open) circles. (d,e) Comparison of amplitude histograms determined by software (d) and the chip (e).

as filled and open circles in Fig 7(b,c). While the spike-amplitudes for the different directions of motion appear to be different, the spike-histogram shows a single broad distribution that is robust to bin-size. Histograms of the spikes corresponding to different stimuli reveal different but overlapping distributions as shown in Fig 7(d,e). Although there may be some overlap between the active neurons and resulting spike characteristics in the two stimulus conditions, in the following figures we assume that the stimuli may be discriminated by the spike features and investigate the discrimination performance for the stimulus condition based on the measured spike features.

In Fig 8(a,b), we plot the spike-peak voltage vs. the spike-trough voltage to show that there appear to be two clusters of spikes in the measurement. The scatter plot suggests that the trough values for the spikes may provide a more robust feature for discriminating the stimulus condition. The histograms of trough value shown in Fig 8(c,d) are better separated for the two stimulus conditions than the amplitude histograms of Fig 7(d,e).

Fig 9 shows a receiver operating characteristic (ROC), i.e. the fraction of true positives versus the fraction of false positives, for both software and hardware detectors. This analysis assumes that a simple threshold detector is used to classify the stimulus condition for each spike according to the single measured feature of interest, amplitude in Fig 9(a) or trough in Fig 9(b). Varying the threshold changes the tradeoff between missed detections and false positives. The percent correct detection for the rightward motion stimulus is plotted versus the percent of false positives; an ideal detector follows the left and top edges of the graph. MATLAB-extracted spike amplitudes are better at discriminating the stimulus condition than chip-extracted spike amplitudes, as indicated by the higher curve in Fig 9(a); the area between the curves indicates the relative performance loss in using the spike amplitude extracted directly on-chip. However, in this case the trough value appears to be a more robust feature for detecting the stimulus condition, and for this feature the MATLAB-extracted trough values and chip-extracted trough values perform equally well, as indicated in Fig 9(b).

To better quantify the amount of error created by the feature detection process, we used a software algorithm to detect and extract the peak and trough voltages from a 2.0 millisecond window following a threshold crossing and compared it to the peak and trough voltages

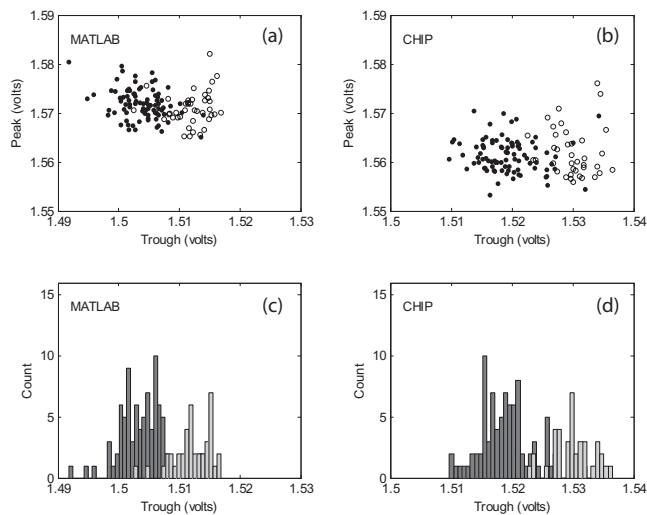


Fig. 8. Top row: Scatter plots from the software and chip measurements. Bottom row: Histograms of the trough detector outputs.

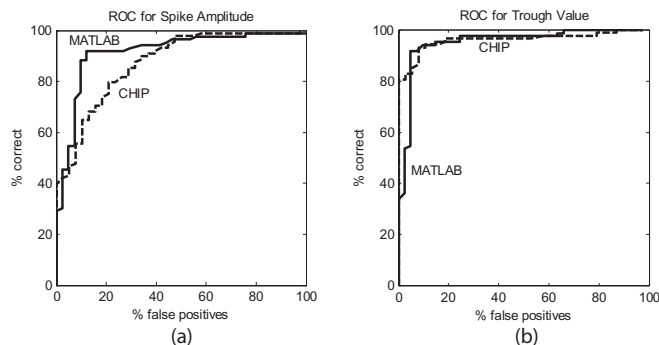


Fig. 9. ROC curve for spike amplitude and trough value for both software and chip features.

obtained from the chip. Fig 10 shows a scatter plot of a representative data set. Due to the relatively high decay rate in the peak detector and the late sampling time of the peak, an underestimate of the amplitude by the chip is expected; this should merely be an offset error that should not affect spike sorting. The signal coupling in the trough detector (discussed earlier) also creates a strong dependence on noise, particularly at low signal levels.

IV. SUMMARY

We have successfully designed, fabricated, and tested a low-power neural amplifier suitable for use in neural recordings, incorporating appropriate filtering and the initial stages of feature extraction useful for subsequent spike-sorting. We demonstrate the use of the chip in a fly recording experiment and show that the chip performs quite well in comparison to a software-based approach, even in challenging spike-sorting situations.

V. ACKNOWLEDGMENT

We thank Jonathan Fritz, Shantanu Ray, and Shihab Shamma for providing the ferret neural recordings. We thank MOSIS for the fabrication of this chip which was used to teach an undergraduate bio-electronics course. T.K.H. is supported by AFOSR (FA95500410188).

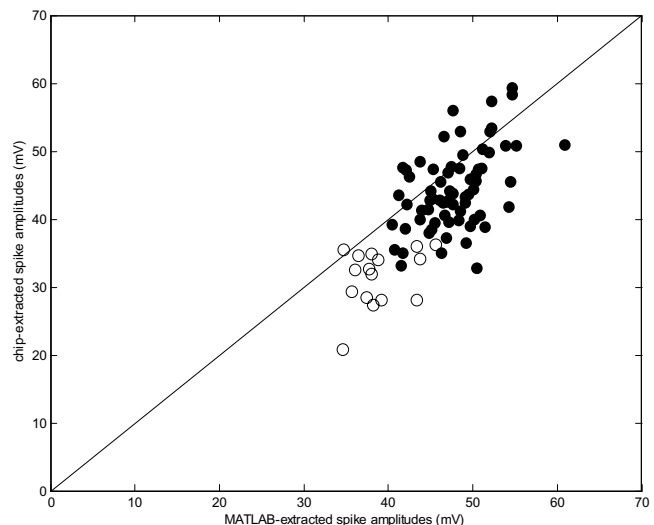


Fig. 10. Spike-by-spike comparison of spike amplitudes extracted by software and by the chip.

This material is based upon work supported by the National Science Foundation under Grant No. 0238061 (P.A.). We thank the UMD MERIT Program for supporting co-authors (D. T. and K. B.) and Tom Swindell and David Sander for their earlier work on this project. We thank Geoffrey Lewen and Rob Harris of Princeton University for their extraordinary generosity in helping us establish a fly recording preparation.

REFERENCES

- [1] R. R. Harrison and C. Charles, *A low-power low-noise CMOS amplifier for neural recording applications*. IEEE J. Solid-State Circuits, vol. 38, pp. 958-965, 2003.
- [2] I. Obeid and J. C. Morizio and K. A. Moxon and M. A. Nicoletis and P. D. Wolf, *Two multichannel integrated circuits for neural recording and signal processing*. IEEE Trans Biomed Eng, vol. 50, pp. 255-8, 2003.
- [3] J. Ramirez-Angulo and C. Urquidi and R. Gonzalez-Carvajal and A. Torralba, *Sub-volt supply analog circuits based on quasi-floating gate transistors*. Intl. Symp. on Circuits and Systems (ISCAS '03), 2003.
- [4] C. Zhang and A. Srivastava and P. K. Ajmera, *A 0.8 V ultra-low power CMOS operational amplifier design*. Midwest Symp. on Circuits and Systems, 2002.
- [5] R. H. Olsson and M. N. Gulari and K. D. Wise, *A fully-integrated bandpass amplifier for extracellular neural recording*. 1st Intl IEEE EMBS Conf. on Neural Engineering, 2003.
- [6] M. Dagtekin and W. Liu and R. Bashirullah, *A multi channel chopper modulated neural recording system*. 23rd Ann. Intl. Conf. of the IEEE Engineering in Medicine and Biology Society, 2001.
- [7] M. Degrauwe and E. Vittoz and I. Verbauwhede, *A Micropower CMOS-Instrumentation Amplifier*. IEEE J. Solid-State Circuits, vol. 20, pp. 805-807, 1985.
- [8] P. Irazoqui-Pastor and I. Mody and J. W. Judy, *In-vivo EEG recording using a wireless implantable neural transceiver*. 1st Intl IEEE EMBS Conf. on Neural Engineering, 2003.
- [9] R. Martins and S. Selberherr and F. Vaz, *A CMOS IC for portable EEG acquisition systems*. IEEE Instrumentation and Measurement Technology Conf. (IMTC/98), 1998.
- [10] T. Horiuchi, T. Swindell, D. Sander, and P. Abshire, *A low power CMOS neural amplifier with amplitude measurements for spike sorting*. Intl. Symp. on Circuits and Systems, vol. 4, pp. 29-32, 2004.
- [11] MATLAB is a registered trademark of The MathWorks, Inc. For MATLAB product information, please contact: The MathWorks, Inc., 24 Prime Park Way, Natick, MA, 01760-1500, USA. Tel.: 508-647-7000; Fax: 508-647-7001; E-mail: info@mathworks.com; Web: http://www.mathworks.com.